COMBINATION OF RANGE PROFILE ALIGNMENT TECHNIQUE WITH AUTOFOCUSING POST – PROCESSING ALGORITHM FOR ISAR IMAGE OPTIMIZATION

E. Kallitsis, A. Karakasiliotis and P. Frangos

National Technical University of Athens
9, Iroon Polytechniou Str., GR 157 73, Zografou, Athens, Greece
Tel: +30 210 772 3694, Fax: +30 210 772 2281, E-Mail: ekalorama@gmail.com, anastasiskarak@yahoo.gr, pfrangos@central.ntua.gr

Abstract

Autofocus is a technique for improving inverse synthetic aperture radar (ISAR) imaging.

In this paper, an autofocusing method is developed for high-resolution stepped-frequency ISAR. Non-uniform rotational motion is compensated through the proposed combination of a conventional coarse range alignment technique and a recently introduced post-processing methodology. In this way, the computa-tional cost of polar reformatting process can be circumvented. The proposed CPI-split autofocusing process results in well focused ISAR images for high angular acceleration periods. Emphasis is placed on further reduction of the computational cost and the storage requirements by applying this post-processing methodology on the range profile history data.

Furthermore, ISAR images entropy dependencies are examined through various simulation results, leading to an acceptable range of entropy values for the autofocusing process.

1. Introduction

Inverse synthetic aperture radar (ISAR) is a kind of a microwave imaging system that exploits signal processing techniques to provide 2-D imaging results for a non-cooperative moving target and can be used for both military and civilian purposes. High bandwidth pulses are transmitted, target echoes at different aspect angles are received and are processed coherently to form the target image. One of the fundamental steps of the ISAR technique is the image focusing or motion compensation [1-8].

In real-world ISAR imaging scenarios, the target being imaged is often engaged in complicated maneuvers and the motion of the target can be divided into translational and rotational motion. The rotational motion contributes to imaging, whereas the transla-tional motion introduces unwanted phase distortion, which is dependent on the target motion parameters [2, 3]. Uniform rotation is necessary to attain efficient cross-range resolution, while non-uniform rotation may significantly degrade the acquired ISAR image quality. Polar reformatting [1] is a multi-step interpolation process to compensate for rotational motion impair-ment, with considerable computational complexity. It is based on rotational motion parameters, which are unknown for non-cooperative radar targets.

In the context of this paper, a range profile alignment technique is combined with an autofocusing post-processing algorithm for ISAR image optimization. Scatterers' migration through resolution cells (MTRC) due to non-uniform rotation [1] can be corrected by the proposed methodology, and ISAR image quality can be improved before further target classification or identification procedures are applied.

Usually, autofocusing is based upon an image entropy minimization criterion [3, 5], which is also adopted in the present study. Alternatively, autofocusing can be achieved via image contrast maximization [6]. In this paper, a conventional coarse range alignment technique, which is based on cross-correlation, is first applied on raw radar data. Following the rotational range migration (RRM) correction, the recently proposed CPI-split autofocusing method [9] is initiated on aligned range profile history data. Small, rapidly maneuvering air targets are the typical ISAR imaging scenario we examine.

Based on an acceptable range of image entropy values, the proposed autofocusing algorithm neglects range profiles leading to poor quality ISAR images. Numerical results validate the image focusing capabi-lity of the proposed method. In order to quantify the ISAR image entropy variation with respect to signal-to-noise ratio, aspect angle and target angular accele-ration, a thorough statistical

analysis is performed based on various Monte-Carlo trials.

In Section 2, we briefly describe the basic points of the proposed autofocusing method, and in Section 3 we present simulation results for a typical ISAR imaging scenario of a fighter aircraft. Finally, useful conclusions are drawn for future research on ISAR image autofocus.

2. Proposed autofocusing algorithm

The conventional range-Doppler technique [1, 2] for ISAR image generation is adopted in the present study. In case of uniform target rotation, polar reformatting process [1] is usually employed to counteract the distortion induced by target rotation (range and cross-range migration) [10]. This process can also be applied to compensate non-uniform rotational motion, but it requires the knowledge of specific kinematic parameters of the target (iterative search for angular velocity and acceleration) and computationally intensive interpolation procedures.

In our study, we assume that the target size does not exceed the practical limit of blur radius [1]. Thus, polar reformatting can be avoided for the case of uniform rotation. In case of non-uniform target rotation (constant angular acceleration), we propose a novel, heuristic autofocusing algorithm to compensate for the ISAR image blurring. The entropy H of the power normalized ISAR image is calculated [8], and, if it exceeds a certain threshold H_{thr}, a post-processing methodology is followed to substitute the received signal part that is affected by the target angular acceleration. Range tracking is also performed through cross-correlation of range profiles with a reference average range profile for the first CPI of the examined ISAR data. Due to RRM restriction in relative aspect angle difference between two range profiles ($\Delta\theta_{RRM} = \Delta r_s / T_D$, where Δr_s is the range resolution and T_D is the target extent) [11], we select to group range profiles (CPI partition) and compute an average range profile for each CPI part, which is cross-correlated with the reference one to derive the required alignment as an integer number of range cells.

The diagram of Fig. 1 depicts the post-processing methodology of the proposed CPI-split autofocusing method [9]. It is based on the partition and the concatenation of the range profile data matrices of two consecutive CPIs.

Naming the CPI during which accelerated rotational motion is exhibited as "unfocused CPI", two different range profile data segments are formed. Concatenated parts of the unfocused CPI and the CPI preceding it ("previous CPI" in Fig. 1) form "segment 1". Similarly, "segment 2" is formed by concatenating parts of the unfocused CPI and the CPI following it ("next CPI" in Fig. 1).

The CPI-split autofocusing method consists of a variable number of stages (N_{stages}), associated with the split depth as a fraction of CPI. In view of hardware implementation cost reduction, the CPI divisor is chosen to be a power-of-two number, increasing by a factor of two from stage to stage. By applying the proposed method on the range profile data, we save the first Fourier transform in conventional range-Doppler imaging and the computational complexity is significantly reduced.

In Fig. 1, the partition and concatenation methodology of the 3rd stage ($CPI/8$) of CPI-split algorithm is graphically depicted. The main concept is the same for all stages of the algorithm ($CPI/2$, $CPI/4$, etc.). The vertical axis of Fig. 1 includes the burst index and the horizontal axis includes the range cell index. Blue and red, numbered ellipsoids indicate respectively the possible data combinations of segment 1 and segment 2. The term combination refers to the concatenation of data parts of two consecutive CPIs. In general, the two data parts to be combined have different sizes in terms of number of bursts, with the exception of $CPI/2$ – stage. Dashed ellipsoids denote those data combinations that are already examined in previous CPI-split stages, which are excluded for an efficient algorithm implementation. The number of possible combinations per segment for the i - th CPI-split stage is

$$N_{i,\,comb} = 2^{i-1} \quad \left(i = 1, \ldots, N_{stages}\right) \tag{1}$$

In our simulations, we set N_{stages} to 4, resulting in a total number of 30 examined data combinations. For each data combination, an ISAR image is formed through two-dimensional Fourier transform and its respective entropy value is computed [8]. At each CPI-split stage, we can either pick the ISAR image with the minimum entropy value or the first ISAR image resulting in an entropy value within an

acceptable range. By setting an appropriate range of acceptable entropy values, the algorithm can be stopped at an early CPI-split stage, saving computational time while still satisfying ISAR image focus criteria.

In order to determine the appropriate values for the entropy threshold H_{thr}, as well as the lower (H_{low}) and upper (H_{upp}) bounds for the acceptable entropy range, we perform various Monte-Carlo simulations to quantify the entropy variation with respect to signal-to-noise ratio (*SNR*), aspect angle and angular acceleration.

In Fig. 2, the probability distribution function (PDF) of the image entropy is plotted for both uniform and non-uniform rotation, for *SNR* equal to 15dB. The angular sector examined is approximately 18.3º, corresponding to 10 CPIs. For the non-uniform rotation case, angular acceleration is set to 0.64 rad/sec^2. These PDF graphs result from 100 Monte-Carlo trials. The first graph provides us with the acceptable entropy bounds, H_{low} and H_{upp}, while the second graph gives us the appropriate entropy threshold H_{thr}.

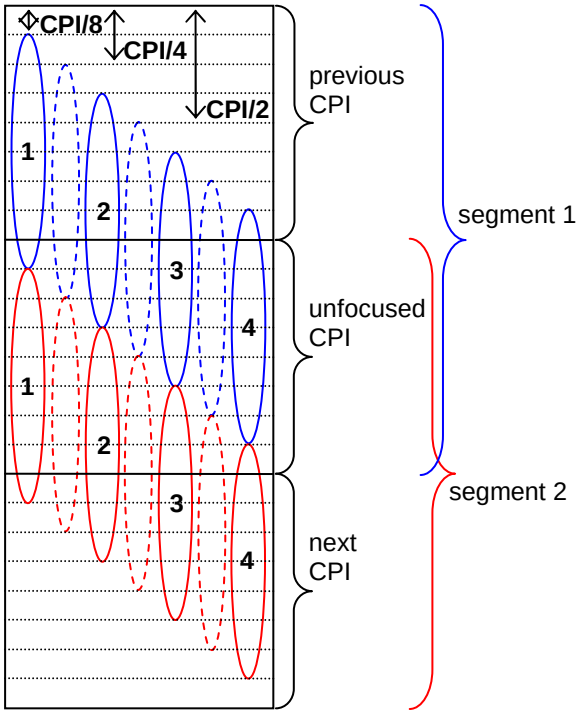

Fig. 1. Post-processing methodology of the proposed autofocusing algorithm: $CPI/8$ – stage

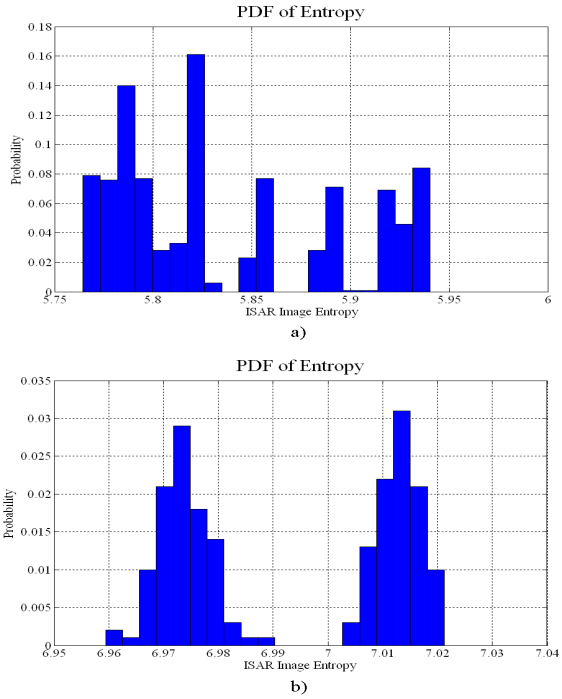

Fig. 2. Probability distribution functions of ISAR image entropy, for *SNR*=15dB: a – uniform rotation; b – non-uniform rotation

3. Numerical results

The simulated target geometry is shown in Fig. 3. It is a point scatterer model of a Mirage 2000C aircraft, consisting of 208 scatterers, with length of 14.5m and wingspan 9.0m. Radar and target motion parameters for our ISAR numerical simulations are included in Table 1.

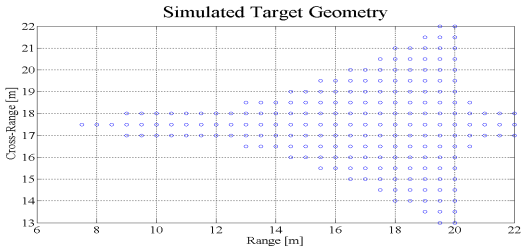

Fig. 3. Geometry of simulated Mirage 2000C target

Table 1. ISAR simulation parameters

Parameter	**Value [units]**
initial carrier frequency, f_0	10 [GHz]
range resolution, Δr_s	0.46875 [m]
cross-range resolution, Δr_c	0.47244 [m]
radar bandwidth, B	320 [MHz]
number of frequencies, M	64
frequency step, Δf	5 [MHz]
pulse repetition frequency, PRF	15 [KHz]
burst duration, T_b	4.266 [msec]
coherent processing interval, CPI	0.546 [sec]
number of bursts, N	128

number of CPIs, N_{CPI}	10
angular velocity, ω	0.0586 [rad/sec]
angular acceleration, γ	0.64 [rad/sec^2]

Backscattered radar data $x(m,n)$ are simulated through the following formula [3]

$$x(m,n)=\sum_{k=1}^{d} s_k \exp\left[-j\frac{4\pi}{c} f_m\left(x_k\cos\theta_n - y_k\sin\theta_n\right)\right]+u(m,n) \quad (2)$$

here d – the number of scatterers; s_k – the scattering intensity of k-th point scatterer; (x_k, y_k) – the Cartesian coordinates of k-th point scatterer, with respect to the radar position; m – the stepped frequency index $(m=1,\ldots,M)$; n – the burst index $(n=1,\ldots,N\cdot N_{CPI})$ for a number of simulated CPIs (N_{CPI}); N – the number of bursts during one CPI; $u(m,n)$ – the two-dimensional additive white Gaussian noise component.

The aspect angle θ_n of the target at slow-time instant t_n is simulated as

$$\theta_n=\begin{cases}\theta_0+\omega t_n+\frac{1}{2}\gamma\left(t_n-t_{start}\right)^2 & , \ angular\ acceleration\ period(s)\\ \theta_0+\omega t_n & , \ otherwise\end{cases} \quad (3)$$

here θ_0 – the initial aspect angle of the target, assumed to be at a distance of 10 Km; ω – the angular velocity; γ – the angular acceleration; t_{start} – the time instant at which an angular acceleration period begins.

In our numerical simulations, N_{CPI} raw data matrices are formed through Eq. (2), assuming uniform rotation, except for particular angular acceleration periods (4th and 8th CPI). Angular acceleration is induced over the specific CPIs through Eq. (3), affecting the respective raw data (rapid angular maneuvers).

The simulated rotational motion profile is shown in Fig. 4, zoomed in the region of the 4th CPI, whose start and end time instants are noted by the blue vertical lines. Time is indexed in units of burst duration (slow-time). Angular variation between uniform and non-uniform rotation periods is smoothed by applying a moving average filter of size $N/8$. The same profile is also simulated for the 8th CPI.

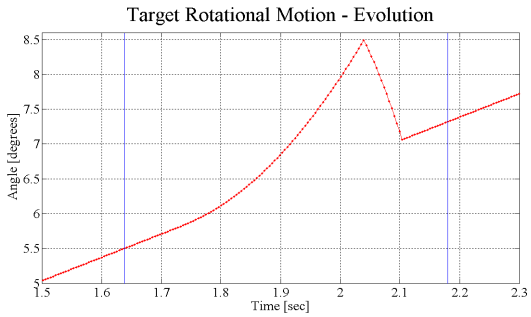

Fig. 4. Simulated rotational motion profile (4th CPI region)

In our simulation scenario, the ISAR images for 10 CPIs are reconstructed through range-Doppler technique, and the entropy values of the power normalized images are computed [8]. For each CPI with image entropy greater than a certain threshold $(H > H_{thr})$, the proposed CPI-split autofocusing algorithm is employed, resulting in a focused image with the minimum entropy over a number of possible data combinations.

ISAR image entropy variation with respect to *SNR* and γ is characterized via 100 Monte-Carlo simulations, carried out for both uniform and non-uniform rotation. Numerical results for entropy variation are shown in Fig. 5. The angular sector scanned is approximately 18.3°, with θ_0 set to 0°. For uniform rotation (angular velocity as in Table 1), strong dependence on *SNR* is observed (for both mean value and standard deviation of image entropy), while the effect of CPI index variation is more obvious for high *SNR* levels. For non-uniform rotation, angular acceleration γ is varied in the range [-0.64, 0.64] rad/sec^2, for *SNR* equal to 15dB and for two specific CPI indices (angular acceleration periods).

The lower and upper bounds for the acceptable entropy range (as a stop condition for the proposed autofocusing methodology) can be determined by a statistical analysis of Monte-Carlo simulation results. For constant angular velocity, we define the ISAR image entropy function with respect to CPI index (n_{CPI}), *SNR* and γ, as $H\left(n_{CPI}, SNR, \gamma\right)$. The entropy bounds that guarantee ISAR image focus are calculated by

$$H_{low}=\min_{n_{CPI}}\left\{\min_{SNR}\left\{H\left(n_{CPI}, SNR, \gamma=0\right)\right\}\right\}-2\cdot\overline{\sigma_H} \quad (4)$$

$$H_{upp}=\max_{n_{CPI}}\left\{\max_{SNR}\left\{H\left(n_{CPI}, SNR, \gamma=0\right)\right\}\right\}+2\cdot\overline{\sigma_H} \quad (5)$$

here $\min_{n_{CPI}}\{x\}$ – the minimum value of x over CPI index; $\min_{SNR}\{x\}$ – the minimum value of x, over all Monte-Carlo trials, for a particular *SNR*; $\overline{\sigma_H}$ – the mean value of the standard deviation of image entropy, over CPI index, for $\gamma = 0$; $2\cdot\overline{\sigma_H}$ – the selected safety margin for the two entropy bounds.

The entropy threshold H_{thr} can be arbitrarily chosen in the range

$$H_{upp} < H_{thr} \le \min_{n_{CPI}}\left\{\min_{SNR}\left\{H\left(n_{CPI}, SNR, \gamma\right)\right\}\right\} - 2\cdot\overline{\sigma_{H,\gamma}} \tag{6}$$

here $\overline{\sigma_{H,\gamma}}$ – the mean value of the standard deviation of image entropy, over CPI index, for the simulated value of γ.

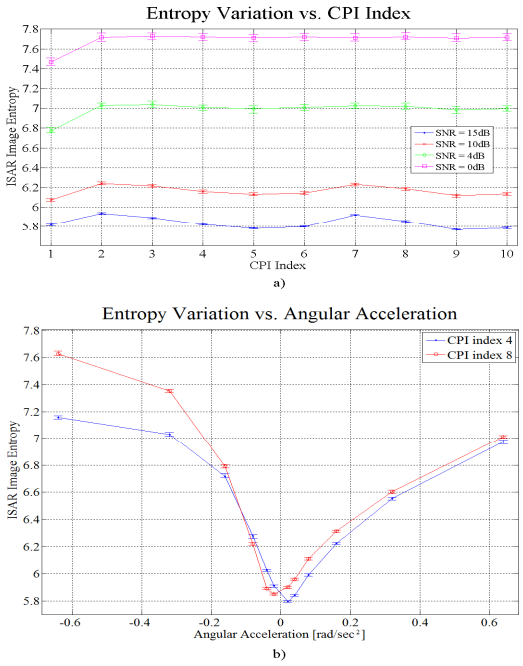

Fig. 5. ISAR image entropy: a – uniform rotation, variation over *SNR* and CPI index; b – non-uniform rotation, variation over *γ*, for specific CPIs and *SNR*=15dB

In Table 2, the selected values of entropy bounds and entropy threshold are cited.

Table 2. Selected entropy bounds and entropy threshold

Algorithm Parameter	Value
lower entropy bound, H_{low}	5.7586
upper entropy bound, H_{upp}	5.9460
entropy threshold, H_{thr}	6.0000

In Fig. 6(a) the average range profile for the 1st CPI is shown. It is used as the reference profile for the cross-correlation based range alignment procedure. Similar average range profiles are computed for each CPI part. In our scenario, $\Delta\theta_{RRM}$ is approximately 1.88°, leading to averaging over the whole CPI in case of uniform rotation and over $CPI/2$ in case of rotational acceleration. In Fig. 6(b) the range profile history for the 8th CPI, after range alignment application, is shown. In Fig. 7, reconstructed ISAR images are presented for *SNR* equal to 15dB and γ set to 0.64 rad/sec² for the 8th CPI. A set of images is included: previous CPI, unfocused CPI, next CPI and unfocused CPI after the application of CPI-split auto-focusing algorithm. We can easily notice that the proposed autofocusing process eliminates the significant ISAR image smearing (Fig. 7, b).

The entropy values for the obtained ISAR images for both 4th and 8th CPI are included in Table 3. Focus improvement is also validated through these results. It is remarkable that the algorithm reaches the optimum combination (minimum entropy) at different CPI-split stages for each unfocused CPI, due to aspect angle variation of image quality.

Table 3. Entropy values for presented ISAR images

ISAR Image Case	Entropy	Minimum Entropy Combination
3rd CPI 4th CPI, Unfocused 5th CPI	5.8814 6.9807 5.7726	
4th CPI, Focused	5.7696	stage 2, segment 1, comb. 1
7th CPI 8th CPI, Unfocused 9th CPI	5.9072 7.0197 5.7563	
8th CPI, Focused	5.7621	stage 4, segment 2, comb. 8

Conclusions

In this paper, an ISAR autofocusing method is developed for small, rapidly maneuvering air targets. Accelerated rotational motion is compensated through the combination of a conventional range alignment technique and the proposed autofocusing algorithm. In this way, the computational complexity of the polar reformatting process can be avoided. Based on ISAR image entropy minimization criterion, the proposed algorithm neglects data leading to ISAR images of poor quality and uses only data

leading to ISAR images of superior quality. Simulation results verify the adaptiveness of the autofocusing procedure to different ISAR imaging conditions. Moreover, the ISAR image entropy variation with respect to aspect angle, signal-to-noise ratio and target rotation parameters is quantified. This is considered to be the first step towards the automation of the proposed autofocusing algorithm, for application to real field data.

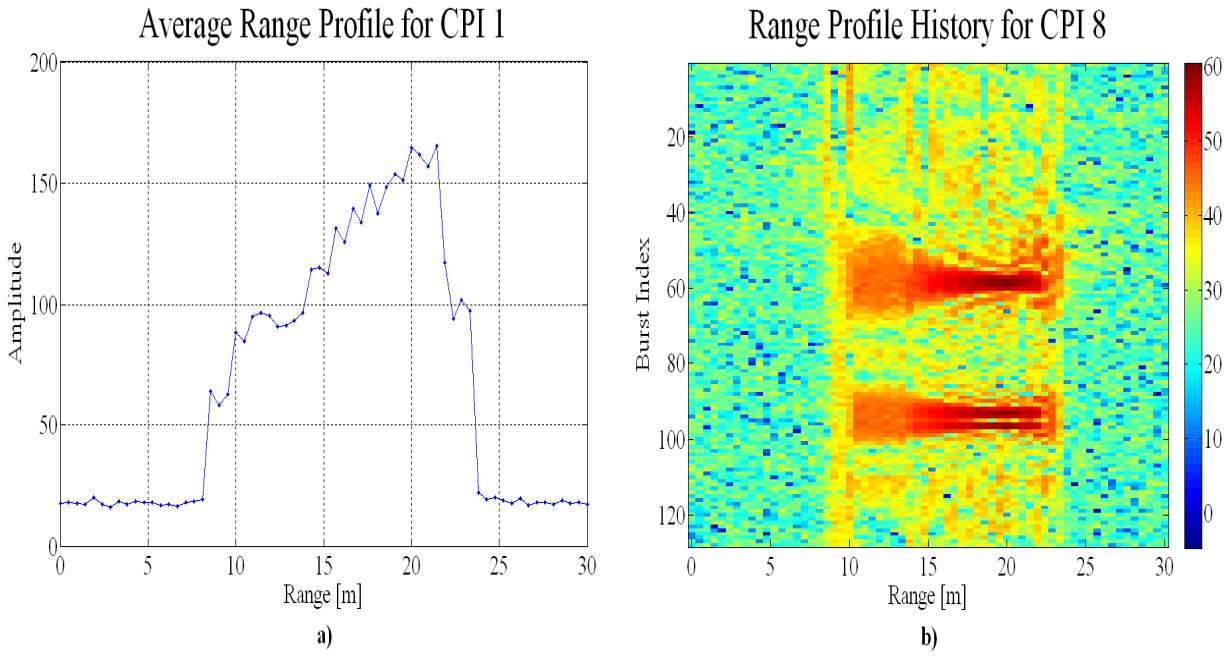

Fig. 6. a – Average range profile for 1st CPI (reference range profile for cross-correlation based range alignment); b – Range profile history for 8th CPI, after range alignment

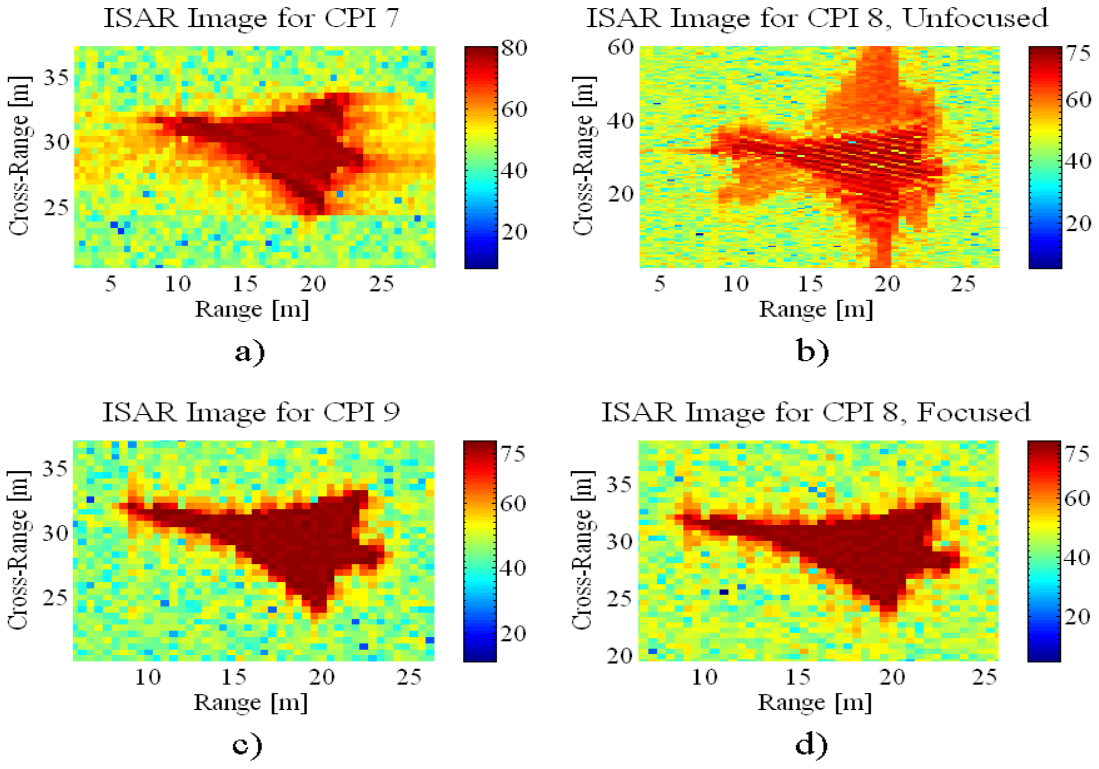

Fig. 7. Reconstructed ISAR images: a – 7th CPI (previous CPI); b – 8th CPI (unfocused CPI); c – 9th CPI (next CPI); d – 8th CPI, after CPI-split autofocusing

References

[1] D. Wehner, High-Resolution Radar, Artech House, 2nd edition, 1995.

[2] V. Chen, and H. Ling, Time-Frequency Transforms for Radar Imaging and Signal Analysis, Artech House, 2002.

[3] Li Xi, Liu Guosui, and Jin Lin Ni, "Autofocusing of ISAR Images Based on Entropy Minimization", IEEE Trans. Aerospace Electron. Systems, Vol. 35, No. 4, Oct. 1999, pp. 1240-1252.

[4] T. Thayaparan, L. Stankovic, C. Wernic, and M. Dakovic, "Real-time motion compensation, image formation and image enhancement of moving targets in ISAR and SAR using S-method based approach", IET Signal Processing, Vol. 2, No. 3, Sept. 2008, pp. 247-264.

[5] A. Lazarov, and C. Minchev, "ISAR Signal Modeling and Image Reconstruction with Entropy Minimization Autofocusing", Proc. DASC, Portland, USA, Oct. 2006, pp. 3E5-1-3E5-11.

[6] M. Martorella, F. Berizzi, and B. Haywood, "Contrast maximization based technique for 2-D ISAR autofocusing", IEE Proc. Radar Sonar Navig., 2005, Vol. 152, No. 4, Aug. 2005, pp. 253-262.

[7] Yu Jizhou, and Jiao Yun, "Research on Motion Compensation Algorithm for Stepped Frequency ISAR Synthetic Aperture Radar", APSAR 2009, Oct. 2009, pp. 626-629.

[8] A. Karakasiliotis, A. Lazarov, P. Frangos, G. Boultadakis, and G. Kalognomos, "Two-dimensional ISAR model and image reconstruction with stepped frequency-modulated signal", IET Signal Proces-sing, Vol. 2, No. 3, Sept. 2008, pp. 277–290.

[9] E. Kallitsis, A. Karakasiliotis, G. Boultadakis, and P. Frangos, "A Fully Automatic Autofocusing Algorithm for Post-processing ISAR Imaging based on Image Entropy Minimization", Electronics and Electrical Engineering Journal, Vol. 110, No. 4, April 2011, pp. 125-130.

[10] S. Wong, E. Riseborough, and G. Duff, "A Numerical Model of ISAR Distortion and an Efficient Procedure for Restoring Distorted ISAR Images", Proc. RTO SET Symposium on Target Identification and Recognition Using RF Systems, Oslo, Norway, Oct. 2004, pp. P2-1-P2-16.

[11] R. van der Heiden, Aircraft Recognition with Radar Range Profiles, PhD Thesis, Univ. Amsterdam, Oct. 1998, p. 47.